A Cardiac Transcriptional Enhancer is Repurposed During Regeneration to Activate an Anti-proliferative Program

Jacob Panten[1], Anna Lubertozzi[2#], Andrew Russell[1#], Jose Segura-Bermudez[1#], Charles Franz[1], Anupama Rao[1], Mateo Zevallos[1], Maciej Pietrzak[3], Kenneth D. Poss[4], and Joseph Aaron Goldman[1*]

[1]Department of Biological Chemistry and Pharmacology, The Ohio State University Medical Center, Columbus OH

[2]Department of Molecular Genetics, The Ohio State University, Columbus OH

[3] Department of Biomedical Informatics, The Ohio State University, Columbus OH

[4]Duke Regeneration Center, Duke University School of Medicine, Durham NC

[#]these authors contributed equally

*corresponding author (aaron.goldman@osumc.edu)

1060 Carmack Rd
Rightmire Hall 105
Columbus, OH 43210
857-600-6488

Abstract:
Previously, we discovered a gene regulatory element, called *103runx1EN* (or *REN*), capable of activating target gene expression throughout the heart during regeneration. REN also drives expression in uninjured cardiac tissue surrounding valves viewed from the reporter and phenotypes arising from a REN-deletion mutant. Activity of the REN reporter peaks just before and during the peak of regeneration. During this time, REN activity in myocardium adjacent to the valves goes away. The expression dynamics of the REN reporter, motifs embedded within REN and the fact that REN activates not just during injury but generally during cardiomyocyte proliferation all suggest that REN is an enhancer promoting regeneration. Unexpectedly, deletion of *REN* results in improved cardiomyocyte proliferation suggesting activation of anti-proliferative factors is part of the normal course of regeneration. REN is also active in the newly formed regenerated muscle during the conclusion of regeneration. Taken together, our findings support a model that in the zebrafish heart, an anti-proliferative gene expression program controls the spatiotemporal dynamics of cardiomyocyte proliferation.

Introduction

Zebrafish have a profound ability to regenerate damaged heart muscle. Heart regeneration proceeds via the proliferation of pre-existing cardiomyocytes (CMs) that replace myocardium lost to injury (Jopling et al., 2010; Kikuchi et al., 2010). Many of the same molecules and pathways required to grow muscle during heart development are reutilized during regeneration (Goldman and Poss, 2020; Huang et al., 2012; Suzuki et al., 2018). However, there are three glaring differences between regeneration and development: the grossly different starting points, the scale of regrowing an adult organ, and how the tissue is able to stop growth once the regeneration is complete. The nearly two decades of research into zebrafish heart regeneration have mainly focused on how regeneration is initiated. Molecules and phenomena have been identified this way. For example, required signaling pathways get activated throughout the heart at early time points and then are focused to the site of injury during the peak of regeneration (Kikuchi and Poss, 2012). The scale difference between regeneration and development may simply be explained with time. (Kikuchi and Poss, 2012) Whereas it takes an embryo 3 days to form roughly ~350 CMs, it takes 30 days to replace at least 10-fold more CMs in the adult. To date, nothing is known about how zebrafish heart regeneration is stopped once muscle has been replaced.

Regeneration is a highly regulated process in its activation, through its peak and very likely at its end. Thousands of genes are changing expression levels in a coordinated, injury-responsive program to drive CM proliferation. Many groups have identified tissue regeneration enhancer elements (TREEs) which can activate target gene expression during regeneration in different model organisms and in different tissue types (Gehrke et al., 2019; Guenther et al., 2015; Harris, 2022; Vizcaya-Molina et al., 2018). In some cases, changes in enhancer activity and tissue specificity have been postulated as underlying the evolution of regenerative capacity. In the case of an enhancer for the Tgfβ ligand *inhba* in zebrafish and killifish, the expression domain viewed from reporters of the enhancer, changed between regenerative organisms like fish to non-regenerative organisms like human (Dogra et al., 2017; Wang et al., 2020). However, the genetic program governing regeneration is likely conserved as several other regeneration responsive enhancers can be utilized to deliver pro-regeneration cargoes in non-regenerative organisms like mammals (Kang et al., 2016; Yan et al., 2022). Like the genes themselves, in some cases regenerative enhancers are reactivated from development and are also required later for regeneration (Harris et al., 2020; Suzuki et al., 2019). While enhancers roles in regulating gene expression during regeneration has been well studied, phenotypes resulting from enhancer deletion have been harder to come by, likely because of the widespread redundancy in regulating gene expression (Bolt and Duboule, 2020). How gene regulation is governed at the end of regeneration is largely unknown.

Previously, to identify regeneration specific genes and regulatory elements, we produced an atlas of nucleosome turnover in the zebrafish heart (Goldman et al., 2017). Using a transgenic histone H3.3, we profiled changes specifically in CMs. Dozens of loci containing enrichment of H3.3 were validated in transgenic reporters assays as enhancers, some of which were exclusive to CMs and others that also stimulated reporter expression in other tissues as well. One such reporter contained a 1265bp region originally found 103kb upstream from the *runx1* locus with H3.3 enrichment that increased during heart regeneration. This *runx1*-linked enhancer (or REN) activated GFP in proliferating cells within the wound of a regenerating heart. REN was not just injury responsive but was also activated in proliferating CMs in a transgenic model of CM hyperplasia where the Nrg1 protein stimulates proliferation rather than injury. Thus, H3.3 profiling in regenerating hearts identified a genetic marker for proliferating CMs.

Here, we further characterize REN and demonstrate how its role unexpectedly changes during regeneration. REN stimulates gene expression in a subdomain of cardiac tissue that surrounds valves leading to the outflow track of the heart. During regeneration, activity around the valve is inversely correlated with REN stimulation in regenerating tissue. We dissected REN into its minimal components

and identified separable regions responsible for expression in different cell types, CMs and epicardium. REN activity peaks just before and during the peak of regeneration, which together with it being a genetic marker of CM proliferation, suggests that REN functions to activate a pro-regenerative gene expression program. Surprisingly, zebrafish mutants with REN deleted have *improved* proliferation of CMs after injury suggesting REN controls an anti-proliferative program. Taken together, this suggests that REN is an enhancer that is repurposed to stimulate gene expression in regenerating tissue.

The REN enhancer activates in cardiac muscle and epicardium.

Previously, we showed that a transgenic reporter containing the REN enhancer cloned upstream of a minimal promoter was able to activate GFP in proliferating cells during heart regeneration (Goldman et al., 2017). REN was first identified using a CM-specific profiling method. This is consistent with *REN:GFP* expression co-staining with an antibody targeting the myosin heavy chain in heart muscle 7days-post-amputation (dpa) (Figure 1A). However, we also observe a significant amount of GFP that is not in the muscle from other cardiac cell-types (Figure 1B). The epicardium, a cell layer enveloping the heart, and endocardium, a second single-cell layer covering the heart lumen are important tissues required for signaling to the myocardium during regeneration (Kikuchi and Poss, 2012; Kikuchi et al., 2011a). To determine whether *REN:GFP* expression also occurs in the epicardium we injured fish containing both *REN:GFP* and *tcf21:mCherry* reporter transgenes and found extensive colocalization in every injured heart (Figure 1CD) (Kikuchi et al., 2011b). Similarly, we tested *REN:GFP* and *flk1:mCherry* double reporter fish for *REN* directed expression in endocardium (Wang et al., 2010). *REN:GFP* activates in a few isolated endocardial cells and not in every heart (Figure 1E). Only a few isolated *REN:GFP* and *flk:mCherry* colocalized cells are detected within the injury area representing less than 1% of the total *flk*-positive cells (Figure 1F, mean 3dpa = 2.0, mean 7dpa = 2.3; N=9,10). We conclude that REN is a regulatory element with predominantly myocardial and epicardial enhancer activity during heart regeneration.

Activation of epicardium (1-3dpa) precedes the peak of CM proliferation (7dpa) during zebrafish heart regeneration (Kikuchi and Poss, 2012). To determine the temporal regulation of REN driven expression we performed a time course on *REN:GFP* reporter fish. The peak of *REN:GFP* expression occurs throughout the heart at 3dpa coinciding with organ-wide activated epicardium (Supp Figure S1A). Total GFP expression organ-wide is slightly decreased at 7dpa and then plateaus by 14 and 21dpa (Supp Figure S1B). Increased expression of GFP at 3dpa reflects a broader distribution of *REN:GFP* positive cells. To measure the potency of transcriptional stimulation we calculated average fluorescence intensity of GFP in colocalized cells. *REN:GFP* intensity did not change in *tcf21:mCherry* cells that colocalized with *REN:GFP* between 3 and 7dpa (Figure 1G, magenta dots, 3dpa: tcf21+GFP average = 20,395; 7dpa: tcf21+GFP average = 24,269; Welch's t-test, $p = 0.4481$). Nor is there any change in average fluorescence intensity in CMs that colocalized with *REN:GFP* (Figure 1G, blue dots, 3dpa:MHC+GFP average = 2770, 7dpa:MHC+GFP average = 2515, Mann-Whitney test, $p > 0.9999$). At 3dpa there is 7.36-fold more GFP intensity in epicardial cells versus CMs and 9.65-fold more GFP intensity at 7dpa, suggesting REN has more potent activity in the epicardium (Figure 1G, 3dpa: Mann-Whitney $p < 0.0001$ N = 15,14, 7dpa: Mann-Whitney $p < 0.0001$, N=10,10). However, we cannot exclude that cell-specific qualities such as size or shape may influence differences in how GFP is localized impacting the observed intensity difference. We conclude that REN:GFP peaks throughout the heart at 3 dpa, is focused at the site of injury by 7dpa, and is brighter in the epicardium than the myocardium.

Expression of GFP in *REN:GFP* reporters is not unique to regeneration. In uninjured hearts, we observe GFP expression in CMs surrounding the valves leading from the ventricle to the outflow tract (Figure 2A). Similar expression was observed in each of the three independent REN reporter lines that we originally generated (Goldman et al., 2017). Besides in CMs, GFP is also observable in non-muscle tissues around the valves. *REN:GFP* marks epicardial cells that emanate above the valve around the outflow tract (Figure 2B). Like during regeneration, *REN:GFP* largely expresses in CMs and epicardium. Interestingly, *REN:GFP* expression disappears in the myocardium surrounding the valve during regeneration at 3dpa and at 7dpa (Figure 2CD). *REN:GFP* expression in valve adjacent muscle begins to return by 21dpa (Supp Figure 2). Since *REN:GFP* has maximal expression in CMs at 3 and 7dpa, we conclude that *REN* regulation of gene expression is inversely correlated between CMs adjacent to valves and CMs that are undergoing regeneration.

Minimal components of REN contain binding motifs for known pro-regeneration transcription factors.

To identify the minimal sequence components that promote REN activity we produced new transgenic reporter lines with sub-fragments of REN cloned upstream of a minimal promoter driving GFP. Previously, we found DNA sequence motifs enriched in regeneration specific H3.3 peaks and ranked them by their specificity to regeneration (Goldman et al., 2017). Using the FIMO analysis tool we searched the REN enhancer for enrichment of these Cardiac Regeneration Motifs (or CRM) and found four clusters of CRM that included some of the most regeneration specific sequences (Supp Figure S2A). Using the four clusters of CRM as a guide, we divided REN into four blocks and made transgenic reporters containing these blocks in different combinations (Figure 3A).

To find a defined minimal fragment responsible for REN epicardial expression we looked for fragments of REN that retained expression in epicardium. A fragment containing an extended region encompassing the first two blocks, called REN-b12+ is sufficient for activating GFP in *tcf21* positive cells (Figure 3B). A second fragment containing just the blocks 1 and 2 called REN-b12 is not able to activate in the epicardium (Figure 3C) nor is the smaller REN-b1x fragment (Figure 3D). Therefore, the 375bp extended region of REN-b12+ beyond blocks 1 and 2 is necessary for epicardial activity. However, a transgenic reporter containing block 2 and the 375bp extended region (b2+) does not activate GFP at all during regeneration. This suggests that the 375bp region is necessary but not sufficient for epicardial GFP activation.

Amputation of the ventricle apex is a standard injury model that is sufficient for full-length REN activity. However, it is possible that more severe injury models would uncover GFP activity from the subfragments of REN that do not activate after amputation. Therefore, we crossed our REN fragments into the transgenic ZCAT cardiac ablation system where Cre induction releases the diptheria toxin stochastically throughout the heart resulting in ablation of up to 60% of CMs (Wang et al., 2011). Most of the REN subfragments that are silent by amputation remain silent during genetic ablation (REN-b34, REN-b2, REN-b2+, Supp Fig. 3B-D). The one fragment that does activate GFP, REN-deuce27, does so in non-CM cells within the heart wall (Supp Figure 3E). The ZCAT transgenic ablation system includes a red transgenic marker so we could not confirm whether these cells are epicardium using our *tcf21* reporter. However, the expression pattern is highly reminiscent of epicardium raising the possibility that the region responsible for REN expression in epicardium is a 140bp fragment that overlaps with REN-deuce27 and REN-b12+. Further investigation will be required to confirm whether this 140bp region directs epicardial expression from REN.

The minimal fragment required for CM expression from REN was more straightforward. The three transgenic fragments containing block 1 are able to drive GFP in CMs at 7dpa (Figure 3E-H). Any fragment of REN that does not have block 1 also does not activate GFP in CMs (Supp Figure 3B-D). The most regeneration specific motif within block 1, CRM17, has homology to binding sites of the AP1 transcription factor complex (JASPAR, $p = .0175$) previously reported to be required for CM proliferation (Beisaw et al., 2020). Therefore, we isolated a 267bp minimal fragment of REN that is both necessary and sufficient for *REN* myocardial activity during regeneration and that contains binding sites for known regulators of CM proliferation.

To determine the minimal component of REN required for expression around valves we looked at REN fragment reporter expression in uninjured hearts. REN fragments b12+ (Figure 3I) and b1x (Figure 3J) both have activity in myocardium surrounding valves in uninjured hearts and the b2+ fragment (Figure 3K) does not. Thus, the same 267bp minimal region of REN that is necessary and sufficient during regeneration is also necessary and sufficient for myocardial expression in uninjured hearts. We conclude that the same region of the genome is repurposed to activate genes in an alternative expression domain during regeneration.

Deletion of REN causes gene expression changes affecting outflow tract valves.

Reporters for enhancers may contain ectopic expression features that do not reflect endogenous expression domains (Bolt and Duboule, 2020). To address the role of REN in its native context rather than from a reporter, we stably deleted a 3,162bp region of the genome encompassing *REN* using CRISPR that we call Δ*REN*. To determine if a feature of the endogenous *REN* locus includes regulation in cardiac tissue adjacent to valves, we performed RNAseq on uninjured hearts from Δ*REN* mutants and their wildtype siblings. There are 435 transcripts whose abundance significantly decreases by 50% and another 492 transcripts whose abundance significantly increases at least 2-fold in uninjured hearts of Δ*REN* mutants (Figure 4A). The differential abundance of mRNA transcripts suggests that REN does indeed regulate gene expression. Likely, the majority of the transcripts with changing abundance are secondary effects of *REN* disruption and are not direct targets. Interestingly, gene ontology analysis of transcripts with increased abundance in Δ*REN* mutants included three members of the AP1 transcription factor complex, *fosab*, *fosb* and *atf3*. Therefore, disruption of *REN* resulted in increased levels of mRNA from a candidate regulator of REN based on motifs present in its minimal functional fragment suggesting that a feedback loop may be inplace regulating REB activity.

Enhancers have been reported to interact with promoters at incredible distances including between different chromosomes (Markenscoff-Papadimitriou et al., 2014). However, promoters and enhancers typically interact within 1Mb ~80% of the time and the largest reported distance of an enhancer cis-regulating a *validated* promoter is 1.7Mb away for the Myc gene in mouse (Bahr et al., 2018; Gasperini et al., 2019; Gasperini et al., 2020). Since the *REN:GFP* reporter suggests that REN is an activator of genes, we looked at the less abundant transcripts as potential direct targets of REN *in vivo*. Of the 435 less abundant transcripts, 25 are encoded by genes found on chromosome 1 with only 5 of the genes found within 1.7 Mb of *REN* (Figure 4A). One of these genes, *adamts1*, encodes an extracellular matrix protein 832kb away from *REN* and regulates cardiac valves by degrading collagen (Hong-Brown et al., 2015). To see if *REN* deletion results in phenotypes associated with *adamts1*, we stained Δ*REN* mutant hearts for collagen using AFOG and compared them to their wildtype siblings (Figure 4B, Supp Figure 4). Uninjured valves surrounding the outflow tract are visibly bluer in Δ*REN* mutant hearts indicating that they have more collagen. Although not conclusive, it does suggest that *adamts1* may be a target of *REN* in uninjured hearts. Taken together, deletion of endogenous *REN* results in decreased abundance of a cardiac valve associated gene *adamts1* with phenotypes in the valve associated with Adamts1 function. We conclude that *REN:GFP* expression around cardiac valves in uninjured hearts reflects endogenous regulation by *REN*.

Deletion of *REN* causes increased CM proliferation.

Multiple lines of evidence suggest that REN is an integral part of a pro-regenerative gene expression program. First, REN is a genetic marker of CM proliferation independent from injury (Goldman et al., 2017). Second, REN activity peaks just before and during the peak of CM proliferation during regeneration (Figure 1). Finally, a minimal fragment of REN that retains activity in CMs also harbors binding sites for transcription factors already shown to be required for regeneration (Figure 3). To address whether REN is an integral part of a regeneration gene regulatory network we tested our Δ*REN* mutants for their ability to complete regeneration. Based on the evidence from the reporter, our expectation was that homozygous mutants lacking the *REN* enhancer would have impaired regeneration. We performed surgeries where we amputated the apex of Δ*REN* mutants and their wildtype siblings and looked if regeneration was complete by 30 days. The Δ*REN* mutants have complete regrowth of cardiac muscle and nearly complete removal of scar indistinguishable from their wildtype siblings (Figure 5AB). We conclude that REN is not necessary to complete regeneration.

While heart regeneration is completed, it is possible that Δ*REN* mutants are delayed and that defects in regeneration are more subtle. To determine an impairment in regeneration, we measured CM

proliferation levels at an earlier time point in Δ*REN* mutants and their wildtype siblings. We costained hearts recovering from amputation of the ventricle apex with Mef2, a marker for CM nuclei, and EdU, a marker of cell proliferation (Figure 5C). Unexpectedly, we find that Δ*REN* mutants has a significant *increase* in CM proliferation compared to wildtype clutchmates (Figure 5D). The fraction of Mef2c positive CMs that are also positive with the proliferation marker EdU is increased by 40.9% at 7dpa (Fig. 5D, mean: wildtype = 8.29% and mutant = 11.68%, p-value = 0.039, N = 17 vs 10). There is no difference in CM proliferation levels between Δ*REN* mutants and wildtype siblings in uninjured hearts (Supp Figure 5A). Also, there is no increase in overall CM numbers in adult Δ*REN* mutant hearts compared to their wildtype siblings (Supp Figure 5B). Thus, we conclude that Δ*REN* mutants have increased levels of CM proliferation that are specific to heart regeneration. This is in stark contrast to our expectations and suggest that REN is inducing expression of an anti-proliferative program.

Since *REN* is a transcriptional enhancer, we expected that its deletion would cause gene expression changes during regeneration like it does in uninjured hearts. RNAseq of Δ*REN* mutant hearts and their wildtype siblings during regeneration show transcripts that were relatively increasing or decreasing in Δ*REN* mutants. We performed linear regression analysis on the 2,036 transcripts changing during regeneration in wildtype hearts and the 2,159 transcripts changing during regeneration in the mutant and find 93 transcripts where the fold-change was different during regeneration comparing wildtype and Δ*REN* mutant hearts (Fig. 5E). There are 44 transcripts where the fold-change is relatively decreased in Δ*REN* mutants (Fig. 5E, blue dots) and another 49 transcripts where the fold-change is relatively increased in the Δ*REN* mutants (Fig. 5E, red dots). Of the 93 transcripts with differential fold-change, 53 had the CM-specific H3.3 in their promoters during regeneration suggesting that these genes are expressed in CMs (Goldman et al., 2017). The promoters of another 9 genes expressing transcripts whose induction changes in Δ*REN* mutants have active chromatin marks but not CM-specific H3.3 suggesting expression in other cell-types besides CMs (Goldman et al., 2017). We conclude that deletion of REN results in dysregulation of gene expression in multiple cell-types during heart regeneration.

Several of the 49 transcripts that increase relatively more during regeneration in Δ*REN* mutants are known regulators of cardiac regeneration. For example, in mice epicardial expression of Fstl1 increases CM proliferation and in Δ*REN* mutants *fstl1a* mRNA is 4X more abundant during regeneration (increased 22.14–fold in Δ*REN* mutants, increased 5.48-fold in wildtype)(Wei et al., 2015). Also, *fibronectin 1a* (*fn1a*) is required for zebrafish heart regeneration and *fn1a* transcripts increases 11.57–fold in Δ*REN* mutants, but only 6.12–fold in wildtype siblings (Wang et al., 2013). Expression of *ankdr1a*, also known as CARP, increases 5.72-fold in Δ*REN* mutants but only 3.70-fold in wildtype regeneration. An enhancer for CARP called *2ankrd1aEN* was found together with *REN* using H3.3 profiling and *2ankrd1aEN* can drive gene expression at the site of injury in both mouse and porcine hearts (Yan et al., 2022). Finally, genes directly linked to cell proliferation are increased in Δ*REN* mutants such as *gins4b* which is involved in DNA replication (increased 70.99-fold in Δ*REN* mutants, increased 8.39-fold in wildtype siblings, residual = 3.35) and *anln* which encodes a protein required for cytokinesis (increased 7.10–fold in Δ*REN* mutants, increased 2.28–fold in wildtype, residual = 1.72) (Oegema et al., 2000; Takayama et al., 2003). The increased induction of pro-regeneration and pro-proliferation genes in Δ*REN* mutants supports our observation of improved proliferation of CMs (Figure 5C).

Transcripts *increasing* in abundance are likely to be secondary effects of *REN* disruption. One would expect a direct target of REN to *decrease* in expression when *REN* is deleted. There were 44 transcripts with increased fold-change in wildtype hearts during regeneration relative to Δ*REN* mutant hearts (Fig. 5E, red dots). However, none of these transcripts are encoded in genes on chromosome 1 with REN. None of the 14 transcripts decreasing in wildtype regeneration that are further reduced in Δ*REN* mutant hearts regeneration are found on chromosome 1 either. Therefore, none of the 93

transcripts that are changing in abundance in *ΔREN* mutant hearts during regeneration are likely to be direct targets of the *REN* regulatory element. Interestingly, included in the transcripts identified as decreasing further in the mutant, are several regulators of sarcomeres. For example, *lmod2a*, regulates thin filament assembly in cardiac muscle (decreases 4.89-fold wildtype, decreases 16.09-fold in Δ*REN* mutants), *tbx5b*, a transcription factor that is known regulator of sarcomeric genes (decreases 3.21-fold in wildtype, decreases 6.98-fold in Δ*REN* mutants), and *mbnl3*, a splicing factor that regulates muscle specific genes (decreases 3.17-fold in wildtype, decreases 7.67-fold in Δ*REN* mutants) all decrease further in Δ*REN* mutants (Ahrens-Nicklas et al., 2019; Basson et al., 1997; Ho et al., 2004; Tsukada et al., 2010). Inhibition of sarcomeric genes is a feature of regeneration (Ben-Yair et al., 2019). The result that several sarcomeric regulators decrease further in Δ*REN* mutant hearts again supports our observation that CM proliferation is increased in Δ*REN* mutants during heart regeneration.

REN is located approximately 103 kb upstream of *runx1*, making *runx1* a possible target of REN. However, we did not detect any reads from transcripts of *runx1* in our RNAseq and therefore no changes in *runx1* abundance in Δ*REN* mutants. Previously, Koth et al. characterized the cardiac-specific phenotypes associated with *runx1* mutants and found that *runx1* mutant hearts exhibit increased CM proliferation similar to Δ*REN* mutants (Koth et al., 2020). One of the main conclusions of Koth et al. was that *runx1* mutants had differential composition of scar after injury that they hypothesize is related to CM proliferation changes. We do not observe similar changes in the abundance of collagen and fibrin in our Δ*REN* mutants. AFOG staining of Δ*REN* mutant hearts is indistinguishable from their wildtype siblings at either 3dpa (Supp Figure 5C) or 7dpa (Supp Figure 5D). We calculated fibrin and collagen within the scars using the methodology described in Koth et al. While we can detect expected differences between scarring at 3dpa and 7dpa there are no differences between Δ*REN* mutants and their wildtype siblings (Supp Figure 5E, 3dpa chi-square p-value = 0.378, Supp Figure 5F, 7dpa chi-square p-value = 0.825). These data point to one of two possibilities. First, that REN does not regulate *runx1* during regeneration or second that CM proliferation increases in *runx1* mutants are unrelated to differences in scaring (please see Discussion for more details).

Activation of an anti-proliferative program would be expected to occur at the end of regeneration when CM proliferation is no longer necessary. Therefore, we looked for *REN:GFP* expression in later timepoints of regeneration within the newly replaced muscle. Indeed, *REN:GFP* expression is found in 21dpa hearts marking the regenerate at roughly 90% the peak intensity observed at 7dpa (Figure 5F). At 30dpa, *REN:GFP* intensity is 63% of what is observed at 7dpa (Figure 5G). The half-life of EGFP is calculated to be 26 hours within live cells and the intensity of GFP does not change much between 7 and 21dpa covering an estimated 9 half-lives (He et al., 2019). This strongly suggests that *REN:GFP* expression at these later time points is an active process and does not reflect the stability of GFP. We conclude that REN is likely activating a gene expression program to curtail CM proliferation at later stages of regeneration.

Discussion

Genetic programs that curtail zebrafish heart regeneration at later stages when it is complete are not well known. Here, we describe a transcriptional enhancer called REN that is active in regenerating cells at early stages but also robustly activates GFP in reporters in the freshly deposited regenerative muscle at the end of regeneration. Targeted removal of this enhancer using CRISPR resulted in increased CM proliferation suggesting it is governing an anti-proliferative program. The REN enhancer also activates genes in uninjured hearts in cardiac tissue around the valves. Disruption of endogenous REN results in increased collagen levels in valve leaflets likely resulting from decreased gene expression. REN driven expression around cardiac valves decreases during regeneration while it is highest at the site of injury suggesting that the enhancer is being repurposed to regulate during regeneration. However, by the end of regeneration, REN activity returns around the valve and is also retained in the newly regenerated muscle. This suggests that while pro-regenerative enhancers are reported to be reactivated from development, those that curb regeneration at its end are repurposed from other pathways.

That the REN enhancer is a genetic marker of CM proliferation *and* activates an anti-proliferative program *in vivo* poses a bit of a paradox. A priori one might expect that a program to stop regeneration would be temporally activated towards the conclusion and not activated nearly simultaneously with regeneration initiation like REN is. However, many signaling pathways, for example activation of Notch or Wnt, display a similar phenomenon where activation of inhibitors of the pathway occurs simultaneously with activation of that pathway. Here, we postulate that the decision for CM to proliferate during regeneration is achieved by a balance of genetic pathways. At early stages of heart regeneration, the balance is tipped to promote CM proliferation by an over determination of pro-growth pathways. At later stages when activation programs begin to dissipate, the balance tips more in favor of the REN pathway to bring CM proliferation to an end. Removal of REN during the peak of regeneration tips the balance further towards proliferation. The lack of major heart growth phenotypes towards the end of regeneration in our Δ*REN* mutants may be a result of redundancy in anti-proliferation programs such that the balance still tips towards halting CM proliferation at the end of regeneration.

We could not conclusively establish direct targets of gene regulation by REN. The gene closest to REN, *runx1*, has interestingly been reported to have a similar increase in CM proliferation when mutated (Koth et al., 2020). This phenotype is not commonly described in zebrafish mutants which are commonly loss of function when it comes to heart regeneration. Together with their proximity, this strongly argues for *runx1* and REN to be in the same genetic pathway. Some differences between REN and runx1 phenotypes exist, however. In mutants for *runx1*, Koth et al. reported changes in scar composition not observed in our REN mutants (Supp Figure 5). This may be partly attributed to the fact that REN is not robustly activated in endocardial cells the way *runx1* is (Figure 1E-F) which suggests that REN regulates *runx1* expression in muscle and epicardium during regeneration and not endocardium. It also suggests that increases in CM proliferation in the *runx1* mutant are not related to observable differences in scaring. Likely, *runx1* functions as an anti-proliferative transcription factor in muscle and/or epicardium possibly by repressing *fstl1a* expression (Figure 5H). In mice, Runx1 is induced in certain models of dilated cardiomyopathy (Kubin et al., 2011) and knockout of *Runx1* in muscle improves recovery after heart injury (McCarroll et al., 2018). However, changes in CM proliferation levels have not been reported to underlie improved cardiac remodeling. Recently, *Runx1* has been reported to be linked to the abundance of more proliferative mono-nucleus diploid CMs (MNDCMs) (González-Rosa et al., 2018; Patterson et al., 2017). We postulate here, that over-expression of Runx1 in early stages of mouse post-natal development increase numbers of MNDCMs by inhibiting proliferation and preventing their binucleation (Swift et al., 2023).

While REN may regulate *runx1* in some cells during regeneration it is unlikely to be doing so in uninjured hearts. The *runx1* BAC reporter, unlike REN, does not show any expression in cardiac tissue

surrounding valves in uninjured hearts (Figure 2) suggesting that REN is regulating different gene(s) in uninjured hearts (Koth et al., 2020).

Most of the heart regeneration field has rightfully focused on discovery of pathways that establish or promote CM proliferation. Such pathways offer the most direct line to therapeutic possibilities. However, in many cases they do not address the major evolutionary and context dependent differences that steer CMs toward proliferation versus hypertrophy. Some of the same molecules that may promote regeneration in zebrafish promote hypertrophy in mammals ((Kikuchi and Poss, 2012)). Repurposing an anti-proliferative program to promote CM proliferation offers an alternative approach where a genetic program present in non-regenerative organisms may be utilized in reverse to bestow regenerative capacity. Such a possibility remains hypothetical. Whether the REN pathway could be remodeled for such a possibility would require knowledge of the direct targets of REN. Future studies extending from the research described here will likely require identifying what promoters REN is interacting with.

Material and Methods

Transgenic fish construction – For reporter fish strains, the regulatory element being studied was cloned upstream of the mouse fos minimal promoter as previously described (Goldman et al., 2017). Stable transgenic zebrafish lines were produced using the I-Sce method of random genomic integration. The *tcf21*:Red reporter and the *flk*:Red reporters were previously published. All zebrafish (*Danio rerio*) used in this study derive from the Ekwill strain. Adults less than 1 year old were used for all the experiments. Males and females were mixed in similar proportions in each of the conditions. All experiments were performed under university supervision according to the institutional animal care and use committee protocol #2018R00000090 of Ohio State University.

Heart injuries – Zebrafish were anesthetized using Tricaine and placed ventral side up on a sponge to carry out resection of the ventricular apex. Iridectomy scissors were used to make an incision through the skin and pericardial sac. Gentle abdominal pressure exposed the heart and ~20% of the apex was removed with scissors, penetrating the chamber lumen (Poss et al., 2002). Hearts were harvested 1, 3, 7, 14, 21 or 30 days after injury depending on the experiment. To genetically ablate CMs, *cmlc2:CreER*^{pd10}*; bactin2:loxp-mCherry-STOP-loxp-DTA*^{pd36} (Z-CAT) fish were incubated in 0.5 µM tamoxifen for 17 h (Wang et al., 2011).

Immunofluorescence – Primary antibodies used in this study were: Rabbit anti-Mef2 (1:100, Abcam, ab197070), Rabbit anti-GFP (1:200, Life Technologies A11122) and Mouse anti-MF20 (1:100, Developmental Studies Hybridoma Bank, MF20). Secondary antibodies were: Goat anti-mouse Alexa Fluor 546 (1:200, Thermo Fisher Scientific, A-11030), and Goat anti-rabbit Alexa Fluor 488 (1:200, Thermo Fisher Scientific, A-11034).

Quantification of fluorescence

Average fluorescence – Briefly, using ImageJ, the red (or blue) channel was thresholded and used to select a region of interest in the green channel where the raw integrated density was calculated. Background was subtracted. The calculated fluorescence was then normalized to area under consideration.

CM proliferation - Injured fish were injected into the abdominal cavity once every 24 h for 3 days (4-6 dpa) with 10 µl of a 10 mM solution of EdU diluted in PBS. Hearts were removed on day 7, embedded and cryosectioned. Slides were stained with Alexa Fluor 594 Azide using click chemistry (Breinbauer and Köhn, 2003) and then immunostained for Mef2c. Briefly, sections were blocked with 1% bovine serum albumin (Fraction V) and 5% goat serum and washed in PBS with 0.2% Triton X-100. Three sections representing the largest wound area were selected from each heart and imaged using a 20× objective. The number of $Mef2^+$ and $Mef2^+EdU^+$ cells were counted using MIPAR image analysis software and the CM proliferation index was calculated as the number of $Mef2^+EdU^+$ cells/total $Mef2^+$ cells (Sosa et al., 2014). The CM proliferation index was averaged across two to four appropriate sections from each heart.

Mutant fish construction - Guide RNAs (sgRNAs) were designed against two regions flanking the REN element on chromosome 1 (sgUpstream: gTA gTg TTg Agg ATA gAC Ag, sgDownstream: gAA AAC AgC TAC AgC TCC CT). DNA templates of the respective sgRNA fused to a tracRNA were produced by PCR. T7-transcribed sgRNA were then injected with Cas9 protein into newly fertilized embryos from EK parents. Mutant strains were genotyped using PCR oligos (Fwd: gCC ACT gCC TCg CCC CTg Cg, Rev: AAT CgA TgA TTC TTg Agg TCA AAg ATg TgT ACT) for the mutant allele. A third oligo (ACA gCT ACA gCT CC TCg gAC) was added to the PCR to identify the wildtype allele. *REN* deletion was perfect without addition of extra nucleotides between the fused cut sites.

RNAseq analysis – Demultiplexed and quality-filtered reads, were aligned to the Danio rerio reference genome GRCz10 using Hierarchical Indexing for Spliced Alignment of Transcripts 2 (HISAT2) (Kim et al., 2015). Read counts for each gene were quantified using featureCounts software (Liao et al., 2014).

Differential gene expression analysis was performed using R package edgeR (McCarthy et al., 2012). The read counts were normalized using TMM method (Robinson and Oshlack, 2010). Differentially expressed genes were selected based on adjusted P value and log2 fold change.

Linear regression analysis - A master list of transcripts was created using the following criteria: (1) The transcript of interest had a P-value<0.05 for both the WT regeneration and Mut regeneration. (2) The transcript of interest had a $\log_2$FC>1 for either WT regeneration or Mut regeneration. Each transcript was assigned its WT regeneration $\log_2$FC as the X-value, and its Mut regeneration $\log_2$FC as the Y-value. A line of best fit was calculated using the master list, and residuals were calculated for each transcripts using the line of best fit. If its residual>1, then the transcript was colored red. If its residual<-1, then the transcript was colored blue.

AFOG staining – Acid Fushin Orange G staining was performed as previously described (Rao et al., 2023). For calculation of relative fibrin and collagen levels we adopted the methodology described in (Koth et al., 2020). Briefly, ImageJ was used to analyze the color of the wound area of sections stained with AFOG. Channels were split and images were color thresholded for red and blue using the same settings for all hearts. Red and blue particles were analyzed and %Area was recorded for each heart. To determine the orange area, %Red and %Blue values were subtracted from 100%. Percents were averaged from at least 5 hearts from each condition.

Statistics - To ensure that experiments were sufficiently powered we used an α error probability of 0.05 and 80% power to calculate if sample sizes were sufficient. For each analysis, we used the Welch's parametric *t*-test to calculate significance. If the variance between the comparison groups was also significant (*F* test for unequal variances), we switched to using a non-parametric test (Mann–Whitney). For the CM counting and CM proliferation assays, one researcher embedded hearts and sectioned slides and a separate researcher who was unaware of the sample identity carried out imaging and quantification.

Figure Legends

Figure 1. The REN enhancer expresses in epicardium and myocardium preceding the peak of regeneration.
(A) Myocardial expression of REN:GFP is shown by staining with Anti-MHC (blue) in hearts 7-days-post-amputation (dpa). (B) MIPAR rendition of colocalization in (A) shows colocalized regions in black and GFP that is not muscle positive in green. (C) Epicardial expression of REN:GFP is shown by colocalization with a *tcf21*:red (pink) reporter in hearts 7dpa. (D) MIPAR rendition of colocalization in (C) shows colocalized regions in black and GFP that is not *tcf21*-positive in green. (E) Endocardial expression of REN:GFP is shown by colocalization with a *flk*:red reporter in hearts 7dpa. (E') MIPAR rendition of flk colocalization from E is shown in black and *flk*-positive cells that are GFP-negative are shown in red. (F) Graph showing numbers of *flk*-positive/GFP-positive cells at 3dpa and 7dpa. (G) Graph showing the normalized GFP fluorescence of REN:GFP colocalized *tcf21*:Red (pink) and muscle (blue) at 3dpa and 7dpa. Zoom of muscle data is shown in the dashed box on the right.

Figure 2: *REN* regulates gene expression in cardiac tissue surrounding valves in uninjured hearts.
(A) Valves around the outflow tract in uninjured hearts are shown by endocardial reporter *flk*:Red (pink). REN:GFP (green) and muscle is stained with MHC (blue). (B) both cardiac muscle (MHC-blue) and epicardium (*tcf21* reporter, pink) colocalize with REN:GFP (green) around uninjured valves. (C-D) Same staining as in (A) but this time on regenerating hearts 3dpa (C) and 7dpa (D).

Figure 3: Myocardial *REN*-directed gene expression is separable from other cell types.
(A) Cartoon represents a map of full-length REN (top green bar) and the seven smaller REN fragments that we tested in stable transgenic reporters. Fragments that induced GFP in epicardium are colored green and fragments that did not induce gene expression from a minimal promoter are colored gray. The epicardial specific region is outlined in a pink dashed box. (B-D) Left – Hearts from the one positive (B) REN b12+ transgenic and the two negative (C) REN b12 and (D) REN b1x reporters at 3-days-post-amputation. Right – MIPAR renditions of colocalized areas are shown in black with excess GFP remaining in green. (E) Same cartoon as in (A) except fragments of REN are colored green based on their colocalization with cardiac muscle (stained with a myosin heavy chain (MHC) specific antibody) 7dpa. (F-H) Left - Hearts from the three positive reporter lines (F) REN b12+, (G) REN b12, and (H) REN b1x Right – MIPAR renditions of colocalized areas are shown in black and white with excess GFP remaining in green. (I-K) Left – Out flow tract regions from uninjured hearts stained with MHC for muscle (blue) and GFP (green). Right – MIPAR renditions of colocalized areas are shown in black and white with excess GFP remaining in green.

Figure 4: *REN* regulates different genes in uninjured hearts and during regeneration.
(A) Volcano plot showing differences in RNAseq from uninjured wildtype hearts vs uninjured Δ*REN* hearts. Transcripts of genes within 1.7Mb of REN on chromosome 1 are highlighted in green and labeled with arrows. (B-C) AFOG staining of uninjured wildtype (B) and uninjured Δ*REN* mutant hearts. Region around the outflow tract valve is shown with a zoom of the valve leaflets on the right.

Figure 5: Deletion of *REN* increases cardiomyocyte proliferation during regeneration. (A) Wildtype and mutant hearts were stained with MHC 30 days-after-amputation. (B) AFOG staining of the same hearts. (C) Images of sectioned amputated ventricles (7dpa) from wildtype and Δ*REN* mutant fish. Sections are stained for Mef2c (green) and EdU (red). Below – double positive cells are highlighted in black using a MIPAR software rendition (Scale bar = 100μm). (D) Quantification of CM proliferation indices (Mef2/EdU double positive over total Mef2 positive) in 7dpa ventricles (average = 8.29% and 11.68%; Welch's t-test, **p-value = 0.039, N = 17 vs 10). Wildtype – blue, mutant – light blue. Horizontal black bars display the mean (middle) or standard error (top and bottom). (E) Scatterplot of RNAseq results comparing wildtype (x-axis) and DREN mutant (y-axis) samples. Each

dot represents a transcript and are plotted by the $\log_2$ for the ratio of normalized reads from regeneration over normalized reads from the uninjured samples. Red dots are those transcripts that deviate by a linear regression >2 and blue dots are those transcripts that deviate by linear regression <-2. (F) Amputated hearts from REN:GFP transgenic fish stained with MHC (blue) 21dpa. (G) Amputated hearts from REN:GFP transgenic fish stained with MHC (blue) 30dpa.

Supplemental Figure Legends

Supp Figure 1 –
(A) Time course of *REN:GFP* expression throughout the heart during regeneration. (Top) REN – green, MHC – blue. (Bottom) – gray scale of REN:GFP. (B) Quantification of total area of GFP fluorescence.

Supp Figure 2 –
(A) Time course of *REN:GFP* -expression around valves to the outflow tract. (Top) REN – green, MHC – blue. (Bottom) – gray scale of REN:GFP.

Supp Figure 3 –
(A) Cartoon of REN with example Cardiomyocyte Regeneration Motifs (CRM) shown from each of the four blocks. (B-E) Heart sections from the different REN fragments (labeled) in ZCAT hearts ablated 7 days-post-induction. Left – gray scale of GFP. Right – MHC (red), REN:GFP (green).

Supp Figure 4 -
(A) AFOG staining of uninjured wildtype (B) and uninjured Δ*REN* mutant hearts. Images are zoomed in on the region around valves near the outflow tract. All replicates are included here to show consistency of the result.

Supp Figure 5 –
(A) Quantification of CM proliferation indices (Mef2/EdU double positive over total Mef2 positive) in uninjured ventricles (wildtype average = 0.78%; mutant average = 0.54%; Welch's t-test, p-value = .252, N = 7 vs 11). Wildtype – blue, mutant – light blue. Horizontal black bars display the mean (middle) or standard error (top and bottom).(B) Graph of total Mef2-positive CM numbers counts in adult uninjured hearts (average = 2095 and 1666; Welch's t-test, p-value = 0.115, N = 7 vs 11). (C) Representative image of injury site from wildtype and mutant hearts 3 days-post-amputation and stained with AFOG (D) Representative image of injury site from wildtype and mutant hearts 7dpa and stained with AFOG. (E) Calculation of relative fibrin (red) and collagen (blue) levels from 3dpa based on Koth et al. methodology. wildtype averages: collagen = 7.75%; fibrin = 8.70%; muscle (orange) = 83.73%; mutant averages: collagen = 5.16%; fibrin = 12.60%; muscle (orange) = 82.25%; Chi-square p-value = 0.3376; N=7,5. (F) Calculation of relative fibrin (red) and collagen (blue) levels from 7dpa based on Koth et al. methodology. wildtype averages: collagen = 1.13%; fibrin = 5.36%; muscle (orange) = 93.51%; mutant averages: collagen = 1.35%; fibrin = 3.89%; muscle (orange) = 93.51%; Chi-square p-value = 0.825; N=5,6.

References

Ahrens-Nicklas, R. C., Pappas, C. T., Farman, G. P., Mayfield, R. M., Larrinaga, T. M., Medne, L., Ritter, A., Krantz, I. D., Murali, C., Lin, K. Y., et al. (2019). Disruption of cardiac thin filament assembly arising from a mutation in LMOD2: A novel mechanism of neonatal dilated cardiomyopathy. *Sci. Adv.* **5**, eaax2066.

Bahr, C., Paleske, L. von, Uslu, V. V., Remeseiro, S., Takayama, N., Ng, S. W., Murison, A., Langenfeld, K., Petretich, M., Scognamiglio, R., et al. (2018). A Myc enhancer cluster regulates normal and leukaemic haematopoietic stem cell hierarchies. *Nature* **553**, 1 27.

Basson, C. T., Bachinsky, D. R., Lin, R. C., Levi, T., Elkins, J. A., Soults, J., Grayzel, D., Kroumpouzou, E., Traill, T. A., Leblanc-Straceski, J., et al. (1997). Mutations in human cause limb and cardiac malformation in Holt-Oram syndrome. *Nat. Genet.* **15**, 30–35.

Beisaw, A., Kuenne, C., Guenther, S., Dallmann, J., Wu, C.-C., Bentsen, M., Looso, M. and Stainier, D. Y. R. (2020). AP-1 Contributes to Chromatin Accessibility to Promote Sarcomere Disassembly and Cardiomyocyte Protrusion During Zebrafish Heart Regeneration. *Circ Res* **126**, 1760–1778.

Ben-Yair, R., Butty, V. L., Busby, M., Qiu, Y., Levine, S. S., Goren, A., Boyer, L. A., Burns, C. G. and Burns, C. E. (2019). H3K27me3-mediated silencing of structural genes is required for zebrafish heart regeneration. *Development* dev.178632.

Bolt, C. C. and Duboule, D. (2020). The regulatory landscapes of developmental genes. *Development* **147**, dev171736.

Dogra, D., Ahuja, S., Kim, H.-T., Rasouli, S. J., Stainier, D. Y. R. and Reischauer, S. (2017). Opposite effects of Activin type 2 receptor ligands on cardiomyocyte proliferation during development and repair. *Nat. Commun.* **8**, 1902.

Gasperini, M., Hill, A. J., McFaline-Figueroa, J. L., Martin, B., Kim, S., Zhang, M. D., Jackson, D., Leith, A., Schreiber, J., Noble, W. S., et al. (2019). A Genome-wide Framework for Mapping Gene Regulation via Cellular Genetic Screens. *Cell* **176**, 377-390.e19.

Gasperini, M., Tome, J. M. and Shendure, J. (2020). Towards a comprehensive catalogue of validated and target-linked human enhancers. *Nat Rev Genet* **21**, 292–310.

Gehrke, A. R., Neverett, E., Luo, Y.-J., Brandt, A., Ricci, L., Hulett, R. E., Gompers, A., Ruby, J. G., Rokhsar, D. S., Reddien, P. W., et al. (2019). Acoel genome reveals the regulatory landscape of whole-body regeneration. *Science* **363**, eaau6173.

Goldman, J. A. and Poss, K. D. (2020). Gene regulatory programmes of tissue regeneration. *Nat Rev Genet* 1–15.

Goldman, J. A., Kuzu, G., Lee, N., Karasik, J., Gemberling, M., Foglia, M. J., Karra, R., Dickson, A. L., Sun, F., Tolstorukov, M. Y., et al. (2017). Resolving Heart Regeneration by Replacement Histone Profiling. *Dev Cell* **40**, 392 404.e5.

González-Rosa, J. M., Sharpe, M., Field, D., Soonpaa, M. H., Field, L. J., Burns, C. E. and Burns, C. G. (2018). Myocardial Polyploidization Creates a Barrier to Heart Regeneration in Zebrafish. *Dev Cell* **44**, 433 446.e7.

Guenther, C. A., Wang, Z., Li, E., Tran, M. C., Logan, C. Y., Nusse, R., Pantalena-Filho, L., Yang, G. P. and Kingsley, D. M. (2015). A distinct regulatory region of the Bmp5 locus activates gene expression following adult bone fracture or soft tissue injury. *Bone* **77**, 31–41.

Harris, R. E. (2022). Regeneration enhancers: a field in development. *Am. J. Physiol.-Cell Physiol.* **323**, C1548–C1554.

Harris, R. E., Stinchfield, M. J., Nystrom, S. L., McKay, D. J. and Hariharan, I. K. (2020). Damage-responsive, maturity-silenced enhancers regulate multiple genes that direct regeneration in Drosophila. *Elife* **9**, e58305.

He, L., Binari, R., Huang, J., Falo-Sanjuan, J. and Perrimon, N. (2019). In vivo study of gene expression with an enhanced dual-color fluorescent transcriptional timer. *Elife* **8**, e46181.

Ho, T. H., Charlet□B, N., Poulos, M. G., Singh, G., Swanson, M. S. and Cooper, T. A. (2004). Muscleblind proteins regulate alternative splicing. *EMBO J.* **23**, 3103–3112.

Hong□Brown, L. Q., Brown, Cr., Navaratnarajah, M. and Lang, C. H. (2015). Adamts1 Mediates Ethanol□Induced Alterations in Collagen and Elastin via a FoxO1□Sestrin3□AMPK Signaling Cascade in Myocytes. *J. Cell. Biochem.* **116**, 91–101.

Huang, G. N., Thatcher, J. E., McAnally, J., Kong, Y., Qi, X., Tan, W., Dimaio, J. M., Amatruda, J. F., Gerard, R. D., Hill, J. A., et al. (2012). C/EBP Transcription Factors Mediate Epicardial Activation During Heart Development and Injury. *Science* **338**,.

Jopling, C., Sleep, E., Raya, M., Martí, M., Raya, A. and Belmonte, J. C. I. (2010). Zebrafish heart regeneration occurs by cardiomyocyte dedifferentiation and proliferation. *Nature* **464**, 606 609.

Kang, J., Hu, J., Karra, R., Dickson, A. L., Tornini, V. A., Nachtrab, G., Gemberling, M., Goldman, J. A., Black, B. L. and Poss, K. D. (2016). Modulation of tissue repair by regeneration enhancer elements. *Nature* **532**, 201 206.

Kikuchi, K. and Poss, K. D. (2012). Cardiac regenerative capacity and mechanisms. *Annu Rev Cell Dev Bi* **28**, 719 741.

Kikuchi, K., Holdway, J. E., Werdich, A. A., Anderson, R. M., Fang, Y., Egnaczyk, G. F., Evans, T., Macrae, C. A., Stainier, D. Y. R. and Poss, K. D. (2010). Primary contribution to zebrafish heart regeneration by gata4(+) cardiomyocytes. *Nature* **464**, 601 605.

Kikuchi, K., Holdway, J. E., Major, R. J., Blum, N., Dahn, R. D., Begemann, G. and Poss, K. D. (2011a). Retinoic acid production by endocardium and epicardium is an injury response essential for zebrafish heart regeneration. *Dev Cell* **20**, 397 404.

Kikuchi, K., Gupta, V., Wang, J., Holdway, J. E., Wills, A. A., Fang, Y. and Poss, K. D. (2011b). tcf21+ epicardial cells adopt non-myocardial fates during zebrafish heart development and regeneration. *Development* **138**, 2895 2902.

Kim, D., Langmead, B. and Salzberg, S. L. (2015). HISAT: a fast spliced aligner with low memory requirements. *Nat. Methods* **12**, 357–360.

Koth, J., Wang, X., Killen, A. C., Stockdale, W. T., Potts, H. G., Jefferson, A., Bonkhofer, F., Riley, P. R., Patient, R. K., Göttgens, B., et al. (2020). Runx1 promotes scar deposition and inhibits myocardial proliferation and survival during zebrafish heart regeneration. *Development* **147**, dev186569.

Kubin, T., Pöling, J., Kostin, S., Gajawada, P., Hein, S., Rees, W., Wietelmann, A., Tanaka, M., Lörchner, H., Schimanski, S., et al. (2011). Oncostatin m is a major mediator of cardiomyocyte dedifferentiation and remodeling. *Cell Stem Cell* **9**, 420 432.

Liao, Y., Smyth, G. K. and Shi, W. (2014). featureCounts: an efficient general purpose program for assigning sequence reads to genomic features. *Bioinformatics* **30**, 923–930.

Markenscoff-Papadimitriou, E., Allen, W. E., Colquitt, B. M., Goh, T., Murphy, K. K., Monahan, K., Mosley, C. P., Ahituv, N. and Lomvardas, S. (2014). Enhancer interaction networks as a means for singular olfactory receptor expression. *Cell* **159**, 543 557.

McCarroll, C. S., He, W., Foote, K., Bradley, A., Mcglynn, K., Vidler, F., Nixon, C., Nather, K., Fattah, C., Riddell, A., et al. (2018). Runx1 Deficiency Protects Against Adverse Cardiac Remodeling After Myocardial Infarction. *Circulation* **137**, 57–70.

McCarthy, D. J., Chen, Y. and Smyth, G. K. (2012). Differential expression analysis of multifactor RNA-Seq experiments with respect to biological variation. *Nucleic Acids Res.* **40**, 4288–4297.

Oegema, K., Savoian, M. S., Mitchison, T. J. and Field, C. M. (2000). Functional Analysis of a Human Homologue of the Drosophila Actin Binding Protein Anillin Suggests a Role in Cytokinesis. *J. Cell Biol.* **150**, 539–552.

Patterson, M., Barske, L., Handel, B. V., Rau, C. D., Gan, P., Sharma, A., Parikh, S., Denholtz, M., Huang, Y., Yamaguchi, Y., et al. (2017). Frequency of mononuclear diploid cardiomyocytes underlies natural variation in heart regeneration. *Nat Genet* **49**, 1346 1353.

Poss, K. D., Wilson, L. G. and Keating, M. T. (2002). Heart regeneration in zebrafish. *Science* **298**, 2188 2190.

Rao, A., Lyu, B., Jahan, I., Lubertozzi, A., Zhou, G., Tedeschi, F., Jankowsky, E., Kang, J., Carstens, B., Poss, K., et al. (2023). The translation initiation factor homolog, eif4e1c, regulates cardiomyocyte metabolism and proliferation during heart regeneration. *Development* **150**, dev201376.

Robinson, M. D. and Oshlack, A. (2010). A scaling normalization method for differential expression analysis of RNA-seq data. *Genome Biol.* **11**, R25–R25.

Sosa, J. M., Huber, D. E., Welk, B. and Fraser, H. L. (2014). Development and application of MIPAR™: a novel software package for two- and three-dimensional microstructural characterization. *Integrating Mater Manuf Innovation* **3**, 123–140.

Suzuki, M., Hayashi, T., Inoue, T., Agata, K., Hirayama, M., Suzuki, M., Shigenobu, S., Takeuchi, T., Yamamoto, T. and Suzuki, K. T. (2018). Cas9 ribonucleoprotein complex allows direct and rapid analysis of coding and noncoding regions of target genes in Pleurodeles waltl development and regeneration. *Dev. Biol.* **443**, 127–136.

Suzuki, N., Hirano, K., Ogino, H. and Ochi, H. (2019). Arid3a regulates nephric tubule regeneration via evolutionarily conserved regeneration signal-response enhancers. *Elife* **8**,.

Swift, S. K., Purdy, A. L., Kolell, M. E., Andresen, K. G., Lahue, C., Buddell, T., Akins, K. A., Rau, C. D., O'Meara, C. C. and Patterson, M. (2023). Cardiomyocyte ploidy is dynamic during postnatal development and varies across genetic backgrounds. *Development* **150**,.

Takayama, Y., Kamimura, Y., Okawa, M., Muramatsu, S., Sugino, A. and Araki, H. (2003). GINS, a novel multiprotein complex required for chromosomal DNA replication in budding yeast. *Genes Dev.* **17**, 1153–1165.

Tsukada, T., Pappas, C. T., Moroz, N., Antin, P. B., Kostyukova, A. S. and Gregorio, C. C. (2010). Leiomodin-2 is an antagonist of tropomodulin-1 at the pointed end of the thin filaments in cardiac muscle. *J. Cell Sci.* **123**, 3136–3145.

Vizcaya-Molina, E., Klein, C. C., Serras, F., Mishra, R. K., Guigó, R. and Corominas, M. (2018). Damage-responsive elements in Drosophila regeneration. *Genome Res* **28**, 1852 1866.

Wang, Y., Kaiser, M. S., Larson, J. D., Nasevicius, A., Clark, K. J., Wadman, S. A., Roberg-Perez, S. E., Ekker, S. C., Hackett, P. B., McGrail, M., et al. (2010). Moesin1 and Ve-cadherin are required in endothelial cells during in vivo tubulogenesis. *Development* **137**, 3119–3128.

Wang, J., Panáková, D., Kikuchi, K., Holdway, J. E., Gemberling, M., Burris, J. S., Singh, S. P., Dickson, A. L., Lin, Y.-F., Sabeh, M. K., et al. (2011). The regenerative capacity of zebrafish reverses cardiac failure caused by genetic cardiomyocyte depletion. *Development* **138**, 3421 3430.

Wang, J., Karra, R., Dickson, A. L. and Poss, K. D. (2013). Fibronectin is deposited by injury-activated epicardial cells and is necessary for zebrafish heart regeneration. *Dev Biol* **382**,.

Wang, W., Hu, C.-K., Zeng, A., Alegre, D., Hu, D., Gotting, K., Granillo, A. O., Wang, Y., Robb, S., Schnittker, R., et al. (2020). Changes in regeneration-responsive enhancers shape regenerative capacities in vertebrates. *Science* **369**, eaaz3090.

Wei, K., Serpooshan, V., Hurtado, C., Diez-Cuñado, M., Zhao, M., Maruyama, S., Zhu, W., Fajardo, G., Noseda, M., Nakamura, K., et al. (2015). Epicardial FSTL1 reconstitution regenerates the adult mammalian heart. *Nature* **525**, 479 485.

Yan, R., Cigliola, V., Oonk, K. A., Petrover, Z., DeLuca, S., Wolfson, D. W., Vekstein, A., Mendiola, M. A., Devlin, G., Bishawi, M., et al. (2022). An enhancer-based gene-therapy strategy for spatiotemporal control of cargoes during tissue repair. *Cell Stem Cell* **30**, 96-111.e6.

Figure 1

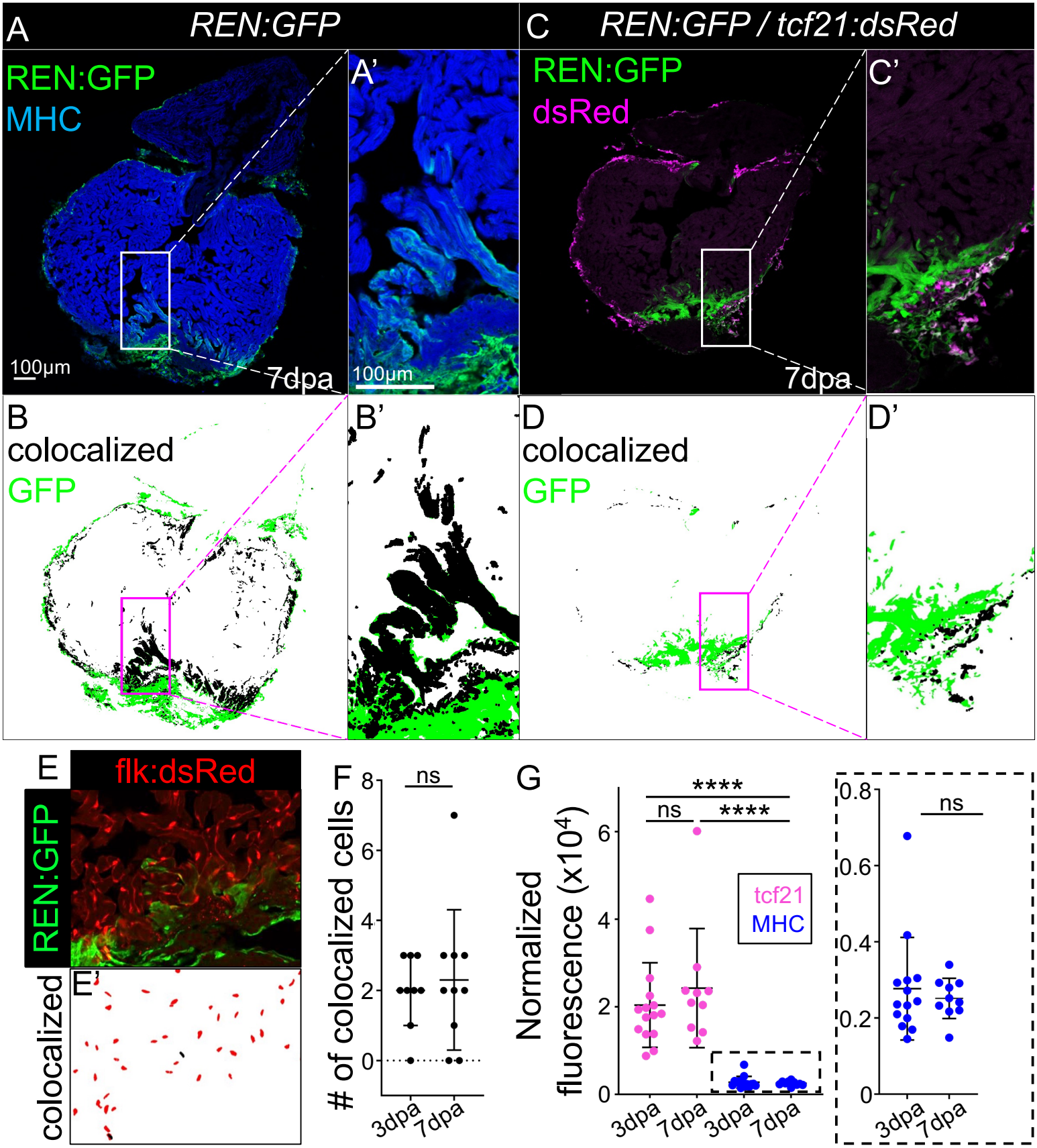
A
REN:GFP
REN:GFP
MHC
100µm
7dpa
A'
100µm
C
REN:GFP / tcf21:dsRed
REN:GFP
dsRed
7dpa
C'
B
colocalized
GFP
B'
D
colocalized
GFP
D'
E
flk:dsRed
REN:GFP
E'
colocalized
F
# of colocalized cells
ns
3dpa
7dpa
G
Normalized fluorescence (x10^4)
****
ns
****
tcf21
MHC
3dpa
7dpa
3dpa
7dpa
ns
3dpa
7dpa

Figure 2

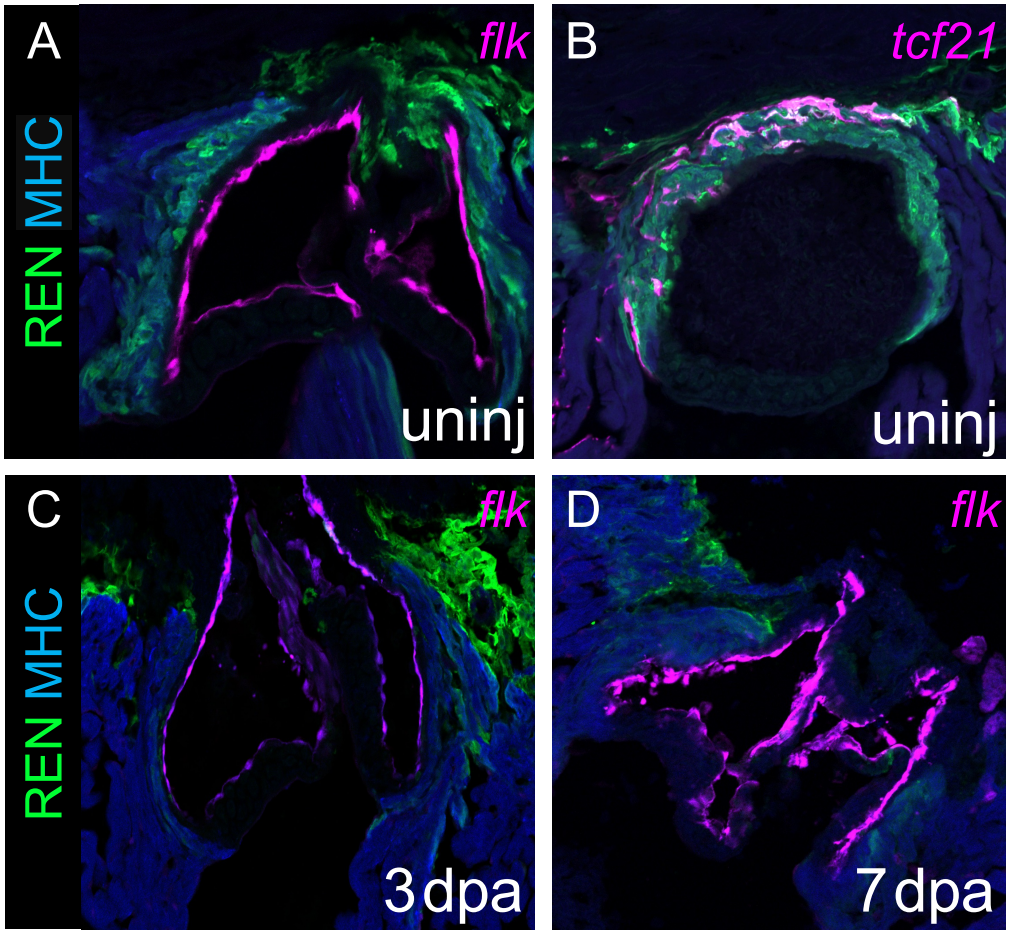

Figure 3

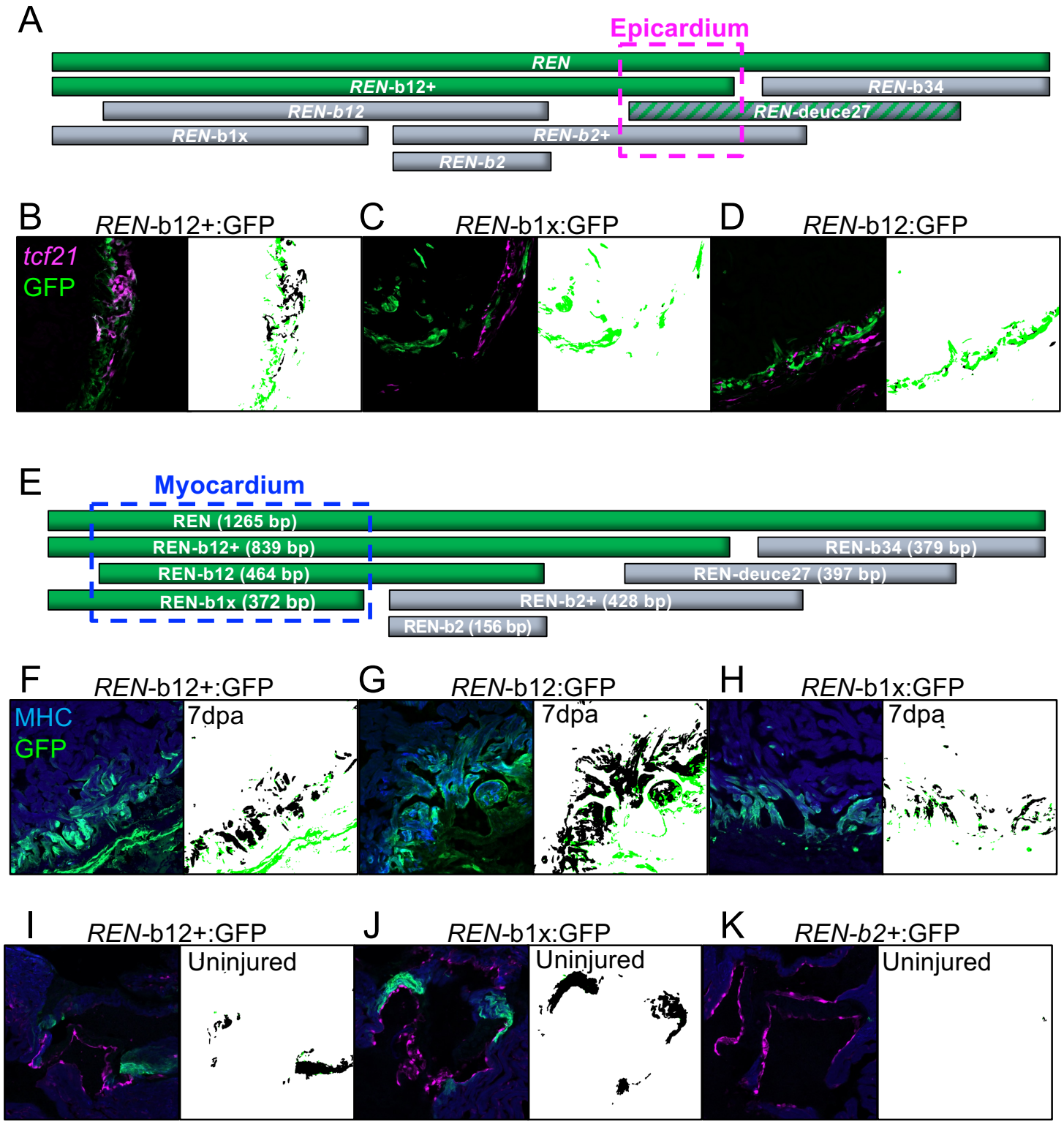
A
Epicardium
REN
REN-b12+
REN-b34
REN-b12
REN-deuce27
REN-b1x
REN-b2+
REN-b2
B
REN-b12+:GFP
tcf21
GFP
C
REN-b1x:GFP
D
REN-b12:GFP
E
Myocardium
REN (1265 bp)
REN-b12+ (839 bp)
REN-b34 (379 bp)
REN-b12 (464 bp)
REN-deuce27 (397 bp)
REN-b1x (372 bp)
REN-b2+ (428 bp)
REN-b2 (156 bp)
F
REN-b12+:GFP
MHC
GFP
7dpa
G
REN-b12:GFP
7dpa
H
REN-b1x:GFP
7dpa
I
REN-b12+:GFP
Uninjured
J
REN-b1x:GFP
Uninjured
K
REN-b2+:GFP
Uninjured

Figure 4

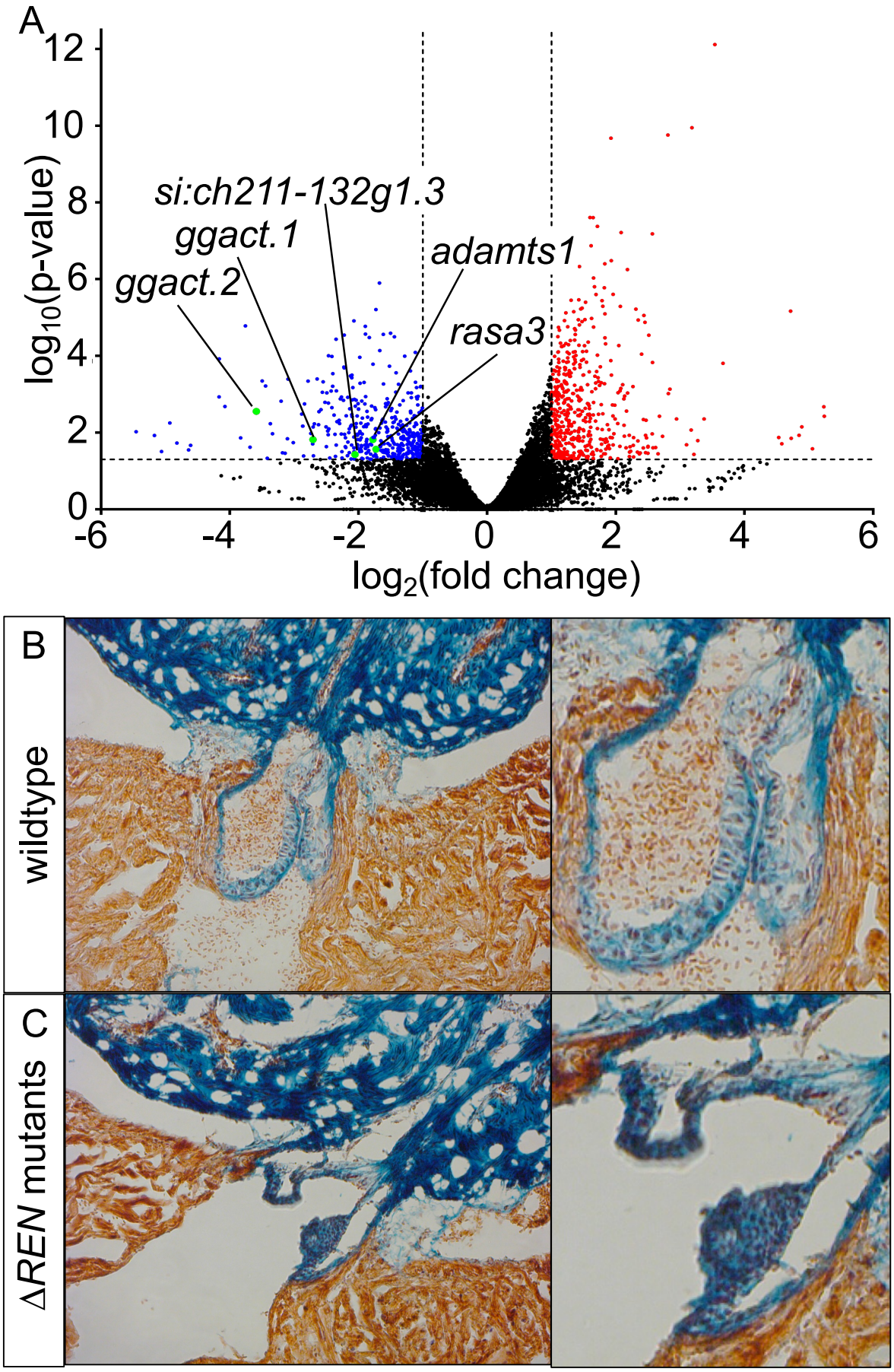
A
12
10
8
6
4
2
0
-6
-4
-2
0
2
4
6
log10(p-value)
log2(fold change)
si:ch211-132g1.3
ggact.1
ggact.2
adamts1
rasa3
B
wildtype
C
ΔREN mutants

Figure 5

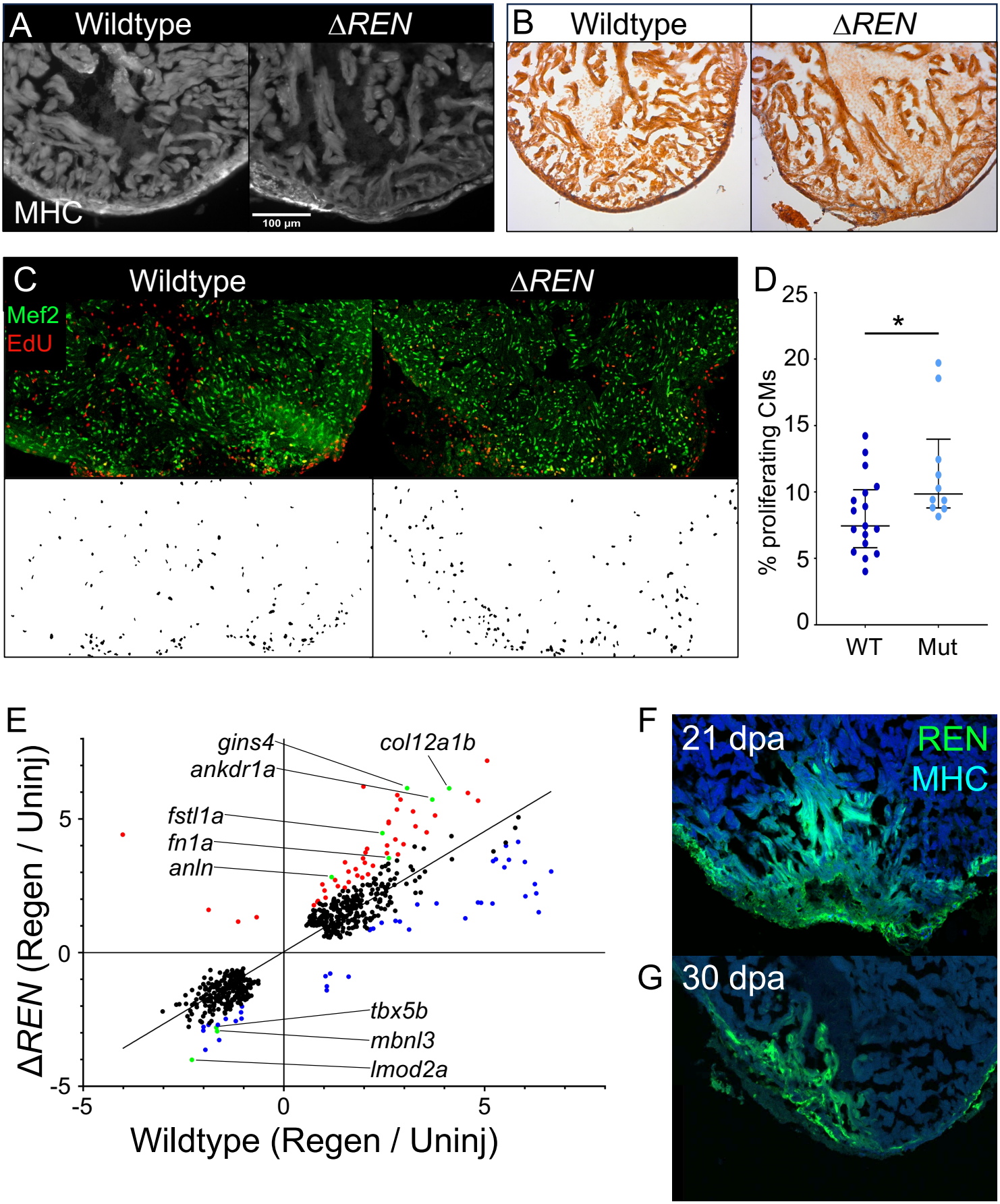
A
Wildtype
ΔREN
MHC
100 µm
B
Wildtype
ΔREN
C
Wildtype
ΔREN
Mef2
EdU
D
% proliferating CMs
25
20
15
10
5
0
*
WT
Mut
E
ΔREN (Regen / Uninj)
Wildtype (Regen / Uninj)
gins4
ankdr1a
col12a1b
fstl1a
fn1a
anln
tbx5b
mbnl3
lmod2a
5
0
-5
-5
0
5
F
21 dpa
REN
MHC
G
30 dpa